Int. J. Heat Mass Transfer. Vol. 27, No. 12, pp. 2355–2364, 1984
Printed in Great Britain

0017–9310/84 $3.00 + 0.00

Natural convection near 4°C in a water saturated porous layer heated from below

KENNETH R. BLAKE and ADRIAN BEJAN
Mechanical Engineering Department, University of Colorado, Boulder, CO 80309, U.S.A.

and

DIMOS POULIKAKOS
Mechanical Engineering Department, University of Illinois at Chicago, Box 4348, Chicago, IL 60680, U.S.A.

(*Received* 23 *April* 1984 *and in revised form* 25 *April* 1984)

Abstract—This paper reports a numerical study of two-dimensional natural convection in a horizontal porous layer heated from below and saturated with cold water. The density maximum of water at 3.98°C and atmospheric pressure occurs inside the layer, as the top surface is maintained at 0°C and the bottom surface is varied from 4 to 8°C. Three separate series of numerical simulations document the effect of Rayleigh number, bottom surface temperature, and horizontal length of the porous layer on the overall heat transfer rate vertically through the layer. The range of these numerical experiments is $200 < Ra_p < 10\,000$, $0.167 < H/L < 1$ and $4°C < T_H < 8°C$, where Ra_p, H/L and T_H are the Darcy-modified Rayleigh number for a fluid with density maximum, the geometric ratio height/length, and the bottom wall temperature. The numerical results agree with published linear stability results regarding the onset of convection.

INTRODUCTION

NATURAL convection in fluid-saturated porous media is a topic that receives considerable attention in the heat transfer literature because of its many engineering applications. Among the engineering activities that benefit from fundamental research on natural convection through porous media are the construction of energy efficient buildings, the extraction of energy from geothermal reservoirs, the design of cooling systems for nuclear reactor cores and windings of electric machinery, and the control of the subterranean water table. In the case of water driven by buoyancy through a porous structure, the flow pattern is influenced dramatically by the occurrence of a density maximum at 3.98°C, if the pressure is atmospheric [1, 2]. Due to the nonlinear relationship between water density and temperature near 3.98°C, the linear Boussinesq approximation [3] commonly used in natural convection analysis is no longer applicable.

A number of studies have dealt already with the effect of density maximum on natural convection in a porous medium saturated with water [4–6]. Of particular interest to the present study are the works of Sun *et al.* [4] and Yen [5], which focused on the onset of natural convection in a porous layer saturated with cold water and heated from below. The objective of the present study is to document numerically the characteristics of natural circulation in a porous layer heated from below, and in this way to verify the linear stability predictions made in ref. [4] regarding the onset of convection. Another objective of this study is to illustrate the high Rayleigh number characteristics of the phenomenon, i.e. the circulation pattern at Rayleigh numbers higher than critical. The water-saturated porous layer considered in this study is a simple model of the moist ground trapped under a layer of ice in winter. However, the same geometry is of great fundamental interest as demonstrated by the literature devoted to the classical problem based on the linear Boussinesq approximation [7–13]. To our knowledge, numerical simulations of natural convection in a porous medium saturated with cold water do not exist: to provide this information is the purpose of the present study.

MATHEMATICAL FORMULATION

Consider a two-dimensional horizontal porous layer saturated with water, as shown schematically in Fig. 1. The layer is bounded above and below by solid walls maintained at temperatures T_C and T_H, where T_H is the bottom temperature and $T_H > T_C$. The boundary temperatures are such that they embrace the density maximum of pure water at atmospheric pressure, $T_C < 3.98°C < T_H$. Unable to study numerically the flow in an infinitely long layer, we select for analysis a section of length L. The geometric aspect ratio of the system is $A = H/L$. The vertical boundaries located at $x = 0$ and L are assumed to be impermeable and adiabatic.

The conservation equations for mass, momentum, and energy for the homogeneous porous medium model [7] are

$$\frac{\partial u}{\partial x} + \frac{\partial v}{\partial y} = 0 \tag{1}$$

$$u = -\frac{K}{\mu}\frac{\partial P}{\partial x} \tag{2}$$

$$v = -\frac{K}{\mu}\left(\frac{\partial P}{\partial y} + \rho g\right) \tag{3}$$

NOMENCLATURE

A	geometric aspect ratio, H/L
c_p	specific heat at constant pressure
g	gravitational acceleration
H	height of porous layer
K	porous medium permeability
l	average horizontal dimension of one roll, equation (19)
L	length of porous layer
n	number of rolls
Nu	overall Nusselt number, equation (16)
P	pressure
Pr	Prandtl number
Q	overall heat transfer rate, equation (17)
Ra_p	Rayleigh number, equation (14)
t	time
T	temperature
T_H	temperature of bottom (hot) boundary
T_C	temperature of top (cold) boundary
u	horizontal velocity
v	vertical velocity
x, y	Cartesian coordinates (Fig. 1).

Greek symbols

α	thermal diffusivity, $k/(\rho c_p)_f$
γ	coefficient, equation (6)
μ	viscosity
ν	kinematic viscosity
ρ	density
σ	heat capacity ratio, equation (5)
ϕ	porosity
ψ	streamfunction.

Other symbols

$( )_f$	fluid
$( )_s$	solid
$(\hat{})$	dimensionless variables of numerical solutions.

$$\sigma\frac{\partial T}{\partial t}+u\frac{\partial T}{\partial x}+v\frac{\partial T}{\partial y}=\alpha\left(\frac{\partial^2 T}{\partial x^2}+\frac{\partial^2 T}{\partial y^2}\right) \quad (4)$$

where the variables u, v, P, ρ, and T are the fluid velocity components, pressure, density, and temperature, respectively. The constants K, μ, and g are the permeability of the porous matrix, viscosity, and gravitational acceleration, respectively. The heat capacity ratio, σ, is defined as

$$\sigma=[\phi(\rho c_p)_f+(1-\phi)(\rho c_p)_s]/(\rho c_p)_f \quad (5)$$

where ϕ is the porosity of the medium and $(\rho c_p)_f$ and $(\rho c_p)_s$ are the heat capacities of the fluid and solid matrix, respectively. Parameter α is the effective thermal diffusivity, defined as $\alpha = k/(\rho c_p)_f$ where k is the thermal conductivity of the porous matrix while saturated with fluid. It is assumed that the fluid is locally in thermal equilibrium with the solid porous structure.

According to Goren [1] and Moore and Weiss [2], the following parabolic relationship between temperature and density may be used within 4% error over the range 0–8°C

$$\rho=\rho_0[1-\gamma(T-3.98°C)^2] \quad (6)$$

where ρ_0 is the maximum density of water at 3.98°C and $\gamma=8\times10^{-6}(°C)^{-2}$. Eliminating the pressure between equations (3) and (4), and incorporating equation (6), leads to the single momentum conservation statement

$$\frac{\partial u}{\partial y}-\frac{\partial v}{\partial x}=-2\frac{K\gamma g}{\nu}(T-3.98°C)\frac{\partial T}{\partial x} \quad (7)$$

where ν is the kinematic viscosity, μ/ρ_0.

To find the steady-state flow and temperature field, the transient evolution of the flow is followed from an initial quiescent and isothermal state $T(x, y) = T_H$. The flow is initiated by changing the top boundary temperature to T_C at time $t = 0$ and maintaining the lower boundary at T_H. The boundary and initial

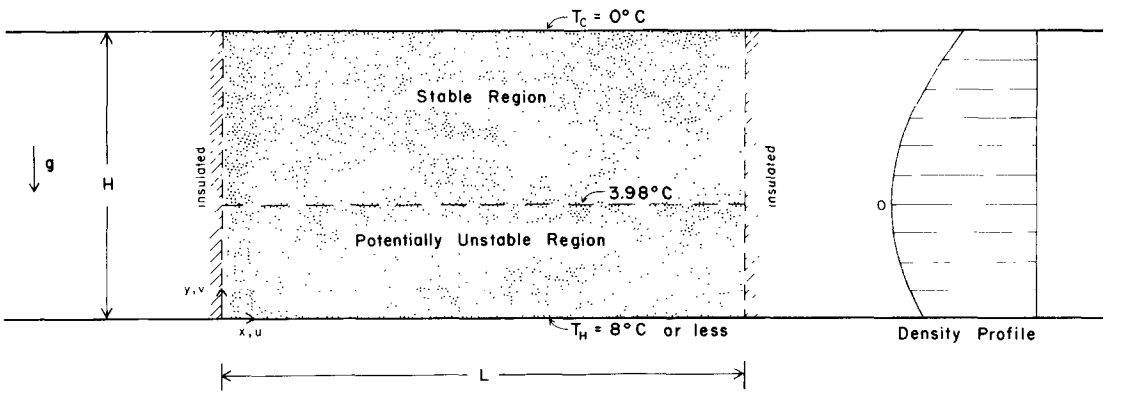

FIG. 1. Two-dimensional porous layer saturated with near-4°C water and heated from below.

conditions are

$$\text{for } t<0: \quad u=v=0, \quad \text{and} \quad T=T_H \quad \text{everywhere}$$

$$\text{for } t\geqslant 0: \begin{cases} v=0, & T=T_H \quad \text{at} \quad y=0 \\ v=0, & T=T_C \quad \text{at} \quad y=H \\ u=0, & \dfrac{\partial T}{\partial x}=0 \quad \text{at} \quad x=0, L. \end{cases} \tag{8}$$

Due to the peculiar form of the density profile, equation (6), the portion of water in the cavity below the point of maximum density is unstably stratified (Fig. 1). Therefore, if Bénard-type flow instabilities begin to develop in the lower portion of the $L\times H$ domain, it is not *a priori* clear what type of temperature and flow patterns will survive in the steady state. In what follows we solve numerically the set of equations (1), (4), and (7) subject to conditions (8), and illustrate the complete flow and temperature fields that prevail in the steady state.

NUMERICAL SOLUTION

Before solving the governing equations it is convenient to cast them in dimensionless form. Defining the following dimensionless variables

$$\hat{x}=x/H, \quad \hat{y}=y/H, \quad \hat{t}=t/(H^2/\nu),$$
$$\hat{u}=u/(\nu/H), \quad \hat{v}=v/(\nu/H), \quad \hat{T}=\frac{T-3.98^\circ\text{C}}{T_H-T_C} \tag{9}$$

and introducing the dimensionless streamfunction $\hat{\psi}$

$$\hat{u}=\partial\hat{\psi}/\partial\hat{y}, \quad \hat{v}=-\partial\hat{\psi}/\partial\hat{x} \tag{10}$$

we can rewrite the governing equations (4) and (7) and the boundary conditions (8) as

$$\left(\frac{\partial^2}{\partial\hat{x}^2}+\frac{\partial^2}{\partial\hat{y}^2}\right)\hat{\psi}=-2\frac{Ra_p}{Pr}\hat{T}\frac{\partial\hat{T}}{\partial\hat{x}} \tag{11}$$

$$\sigma\frac{\partial\hat{T}}{\partial\hat{t}}+\frac{\partial}{\partial\hat{x}}(\hat{u}\hat{T})+\frac{\partial}{\partial\hat{y}}(\hat{v}\hat{T})=\frac{1}{Pr}\left(\frac{\partial^2}{\partial\hat{x}^2}+\frac{\partial^2}{\partial\hat{y}^2}\right)\hat{T} \tag{12}$$

$$\text{for } \hat{t}<0; \quad \hat{u}=\hat{v}=\hat{\psi}=0, \quad \hat{T}=\hat{T}_H \quad \text{everywhere}$$

$$\text{for } t\geqslant 0; \begin{cases} \hat{\psi}=0, & \hat{T}=\hat{T}_H \quad \text{at} \quad \hat{y}=0 \\ \hat{\psi}=0, & \hat{T}=\hat{T}_c \quad \text{at} \quad \hat{y}=1 \\ \hat{\psi}=0, & \dfrac{\partial\hat{T}}{\partial\hat{x}}=0 \quad \text{at} \quad \hat{x}=0, A \end{cases} \tag{13}$$

where Ra_p is a modified Rayleigh number for a porous medium saturated with a fluid having a density maximum

$$Ra_p=K\gamma g(T_H-T_C)^2H/\alpha\nu \tag{14}$$

and Pr is the Prandtl number, $Pr=\nu/\alpha$.

For all the reported results the temperature of the top boundary was set at $T_C=0^\circ$C. The bottom temperature, T_H, was varied from 4 to 8°C. The Prandtl number, held constant at $Pr=11.573$, was calculated for pure water at 3.98°C from the tables in the *Handbook of Chemistry and Physics* [14].

The governing equations (10)–(12) were discretized using the control volume formulation given by Patankar [15]. The region of interest was covered with an array, $m-2$ by $n-2$, of square control volumes. The four boundaries were covered with control volumes of zero thickness. The power-law scheme was used to determine both the heat and mass fluxes across each of the control volume boundaries. It was found that 22 vertical control volumes, including both boundary control volumes, were sufficient to provide accurate results (Fig. 2). The number of horizontal control volumes depends on the aspect ratio, for example an aspect ratio of 1/2 requires 42 horizontal control volumes (see Table 1). The dimensionless time step which gave fast convergence for the majority of cases was $\hat{t}=0.1$.

An iterative process was employed to find the streamfunction from equation (11), the velocity components from equation (10), and the temperature from equation (12). This process was repeated until

$$\frac{\sum_{i=1}^{m}\sum_{j=1}^{n}|\phi_{i,j}^{r+1}-\phi_{i,j}^{r}|}{\sum_{i=1}^{m}\sum_{j=1}^{n}|\phi_{i,j}^{r+1}|}<10^{-6} \tag{15}$$

where ϕ refers to $\hat{\psi}$ or $\hat{T}$, and r denotes the number of time steps.

The effect of fluid motion on the heat transfer between the two horizontal walls of the water saturated porous layer was evaluated by computing the conduction-referenced Nusselt number

$$Nu=\frac{Q}{kL(T_H-T_C)/H} \tag{16}$$

where k is the conductivity of the water saturated porous matrix and Q the overall heat transfer rate defined as

$$Q=-k\int_0^L\left(\frac{\partial T}{\partial y}\right)_{y=0}\mathrm{d}x. \tag{17}$$

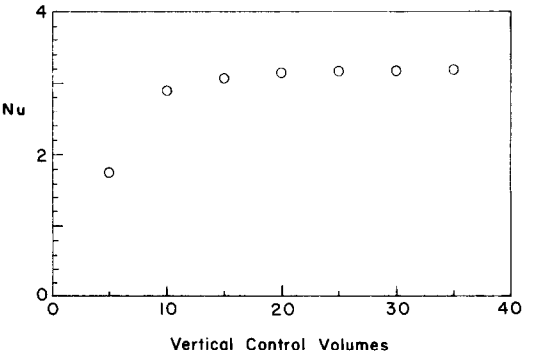

FIG. 2. The influence of mesh size on the accuracy of overall heat transfer rate estimates ($A=0.5$, $T_H=8^\circ$C).

Table 1. Summary of numerical experiments and heat transfer results

Mesh size	Ra_p	T_H(°C)	A	Relaxation factor	Nu	Number of rolls
7 × 12	1000	8	0.5	1.1	1.77	2
12 × 22	1000	8	0.5	1.1	2.85	4
17 × 32	1000	8	0.5	1.2	3.07	4
22 × 42	1000	8	0.5	1.3	3.14	4
27 × 52	1000	8	0.5	1.2	3.17	4
32 × 62	1000	8	0.5	1.2	3.17	4
37 × 72	1000	8	0.5	1.2	3.20	4
42 × 82	1000	8	0.5	1.2	3.20	4
22 × 42	200	8	0.5	1.3	1.00	
22 × 42	250	8	0.5	1.3	1.07	4
22 × 42	300	8	0.5	1.3	1.29	4
22 × 42	500	8	0.5	1.3	2.03	4
22 × 42	1000	8	0.5	1.3	3.14	4
22 × 42	2000	8	0.5	1.2	4.25	4
22 × 42	2300	8	0.5	1.1	4.48	4
22 × 42	2400	8	0.5	1.1	4.56	4
22 × 42	2500	8	0.5	1.1	4.63	4
22 × 42	2600	8	0.5	1.1	5.16	6
22 × 42	3000	8	0.5	1.1	6.49	6
22 × 42	5000	8	0.5	1.1	6.60	6
22 × 42	10000	8	0.5	1.0	7.78	6
22 × 42	1000	8	0.5	1.3	3.14	4
22 × 42	1000	7	0.5	1.3	2.32	4
22 × 42	1000	6	0.5	1.3	1.40	4
22 × 42	1000	5.8	0.5	1.3	1.14	4
22 × 42	1000	5.7	0.5	1.3	1.00	
22 × 42	1000	5.5	0.5	1.3	1.00	
22 × 42	1000	5	0.5	1.3	1.00	
22 × 22	1000	8	1	1.3	1.99	4
22 × 32	1000	8	0.667	1.3	3.01	4
22 × 42	1000	8	0.5	1.3	3.14	4
22 × 52	1000	8	0.4	1.3	3.03	4
22 × 62	1000	8	0.333	1.3	2.77	4
22 × 72	1000	8	0.286	1.2	3.10	8
22 × 82	1000	8	0.25	1.2	3.07	8
22 × 92	1000	8	0.222	1.2	3.09	8
22 × 102	1000	8	0.2	1.1	3.08	10
22 × 122	1000	8	0.167	1.1	3.09	12
22 × 42	300	7.0	0.5	1.3	1.000	
22 × 42	300	7.5	0.5	1.3	1.017	4
22 × 42	500	6.0	0.5	1.3	1.000	
22 × 42	500	6.5	0.5	1.3	1.002	4
22 × 42	500	7.0	0.5	1.3	1.434	4
22 × 42	3000	5.0	0.5	0.8	1.000	
22 × 42	3000	5.5	0.5	0.8	1.806	4
22 × 42	3000	6.0	0.5	1.0	2.514	4

In terms of dimensionless quantitites, the Nusselt number definition reads

$$Nu = -A \int_0^{A^{-1}} \left(\frac{\partial \hat{T}}{\partial \hat{y}} \right)_{y=0} \mathrm{d}\hat{x}. \qquad (18)$$

Equation (18) was integrated numerically after the final temperature field was obtained. A relation similar to equation (18) is obtained by integrating the heat flux along the cold wall situated at $\hat{y} = H$. This second Nusselt number calculation was carried out, and the results were found to be sufficiently close to the values yielded by equation (18) (see Fig. 3).

The two Nusselt number calculations were also used as an additional check on the convergence of the numerical solution. Figure 3 shows the evolution of the top- and bottom-wall Nusselt numbers as the number of iterations increases. In the beginning of the iterative process, the top-wall Nusselt number is very large because the initial temperature of the medium (T_H) differs from that of the upper wall (T_C), equations (8). For the same reason, the starting value of the bottom-wall Nusselt number is zero. The two Nu values approach one another in oscillatory fashion. In all the cases considered in this study the total number of iterations made necessary by criterion (15) was in the vicinity of 400 which is a number considerably greater than the number of iterations required for the two Nusselt numbers to converge, as shown in Fig. 3.

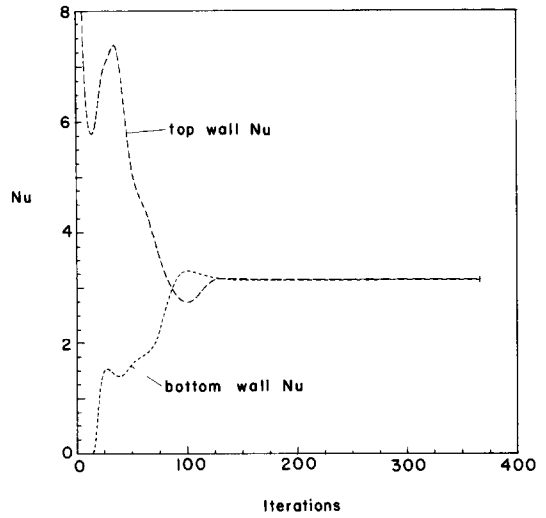

FIG. 3. Top and bottom Nusselt number comparison as test of convergence to the steady state ($A = 0.5$, $T_H = 8°C$, $Ra_p = 1000$).

RESULTS AND DISCUSSION

Table 1 summarizes all the numerical experiments carried out in this study. These numerical simulations were selected in order to investigate systematically the effect of changing one flow parameter at a time. The natural convection phenomenon is influenced by three parameters, the Rayleigh number Ra_p, the bottom wall temperature T_H, and the geometric aspect ratio of the finite domain chosen for numerical analysis, $A = H/L$. The effect of each of these parameters is illustrated in this section.

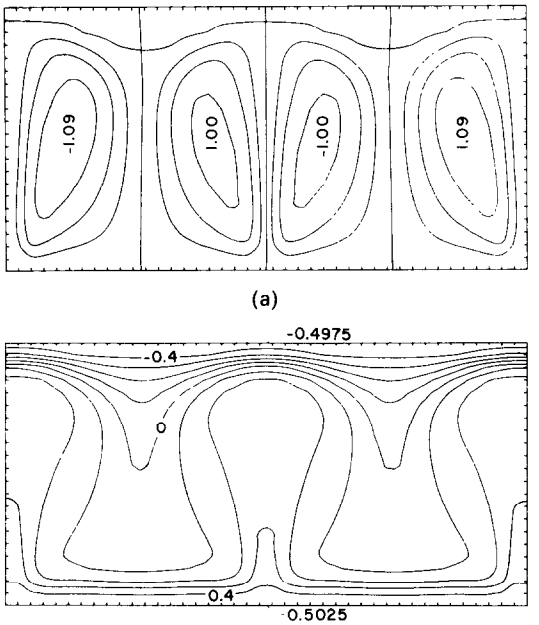

FIG. 5. Numerical solution for $A = 0.5$, $T_H = 8°C$, $Ra_p = 2500$: (a) streamlines ($\hat{\psi} = \text{const.}$); (b) isotherms ($\hat{T} = \text{const.}$).

The effect of Rayleigh number

Figures 4–6 show the flow and temperature patterns in a layer with fixed bottom wall temperature ($T_H = 8°C$) and fixed geometric aspect ratio ($A = 0.5$). The flow is multicellular, and the actual number of cells depends on the Rayleigh number. It is worth

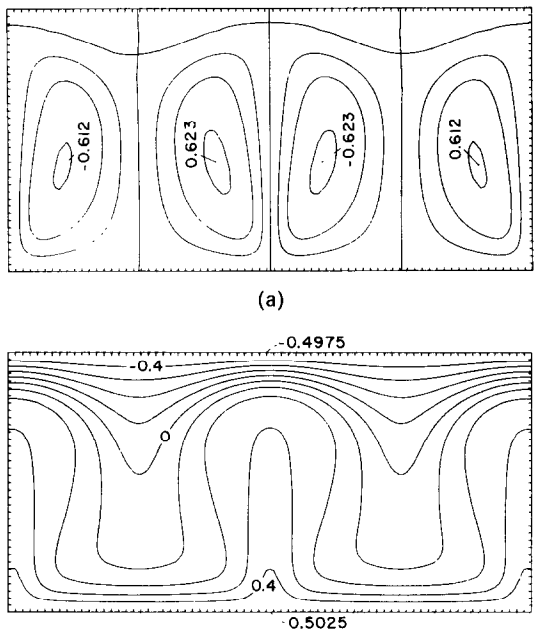

FIG. 4. Numerical solution for $A = 0.5$, $T_H = 8°C$, $Ra_p = 1000$: (a) streamlines ($\hat{\psi} = \text{const.}$); (b) isotherms ($\hat{T} = \text{const.}$).

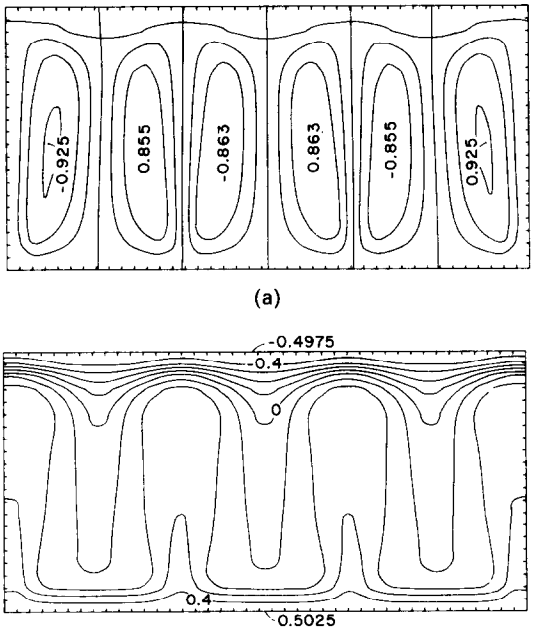

FIG. 6. Numerical solution for $A = 0.5$, $T_H = 8°C$, $Ra_p = 2600$: (a) streamlines ($\hat{\psi} = \text{const.}$); (b) isotherms ($\hat{T} = \text{const.}$).

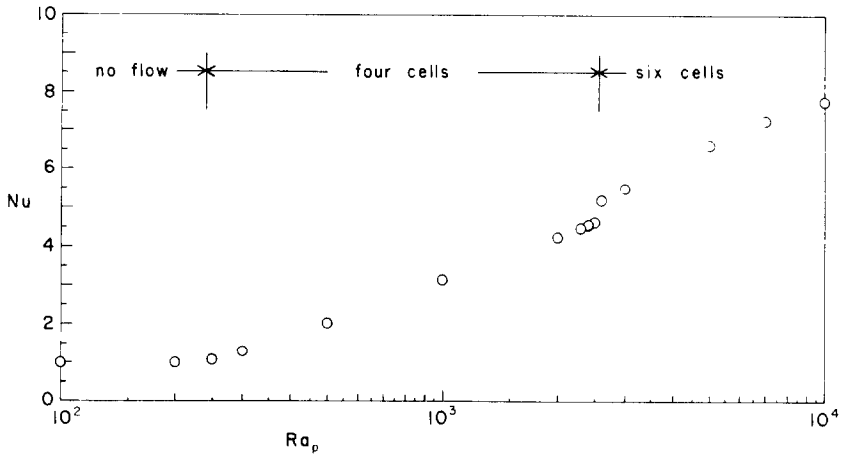

FIG. 7. The effect of Rayleigh number on the overall Nusselt number ($A = 0.5$, $T_H = 8°C$).

noting that to vary Ra_p while keeping T_H and A fixed means to vary the physical depth of the water-saturated porous layer, H.

As Ra_p increases from 1000 in Fig. 4 to 2500 in Fig. 5, the number of cells does not change, however, each cell nearly doubles its flow rate. The centers of all the cells are located in the lower half of the porous layer, i.e. in the region saturated with water heated unstably from below. Near the top boundary of the porous layer the fluid is thermally stratified and practically motionless, despite the strong Bénard-type circulation that intrudes into the upper half of the layer.

An interesting incident of cell multiplication takes place as Ra_p increases from 2500 in Fig. 5 to 2600 in Fig. 6. The number of cells increases from 4 to 6 rather abruptly, and this change is marked also by a sharp jump in the steady-state Nusselt number, as shown in Table 1 and Fig. 7. The effect of cell multiplication on

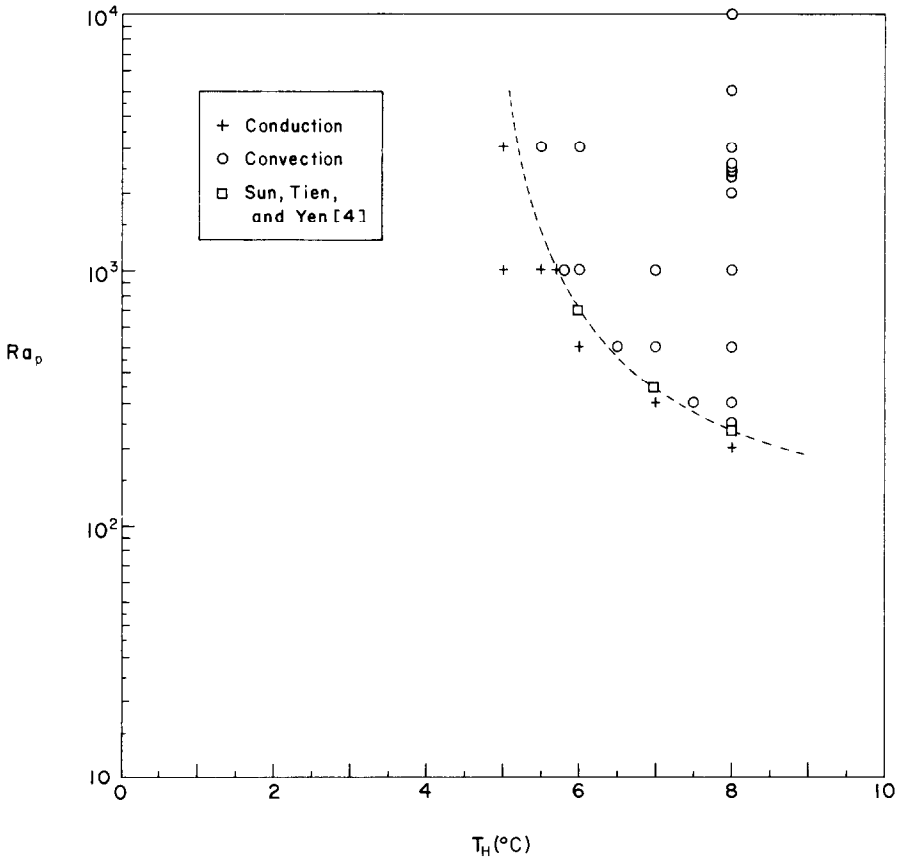

FIG. 8. The frontier between states of pure conduction and convection, showing agreement with the linear stability theory of ref. [4] ($A = 0.5$, $T_C = 0°C$).

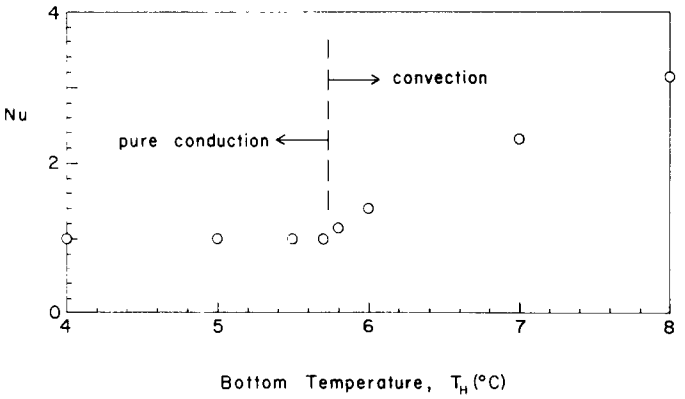

FIG. 9. The effect of bottom temperature T_H on the overall Nusselt number ($A = 0.5$, $Ra_p = 1000$).

the Nusselt number is investigated in greater depth later in this section. In the present series of experiments (Figs. 4–7) we found that as Ra_p increases from 2600 to 10^4 the number of cells remains fixed at 6. We also found that when the number of cells is constant the Nusselt number increases smoothly as the Rayleigh number increases.

Table 1 shows that in a porous layer sandwiched between $T_C = 0°C$ and $T_H = 8°C$ the onset of natural convection takes place at a Rayleigh number Ra_p between 200 and 250. This finding validates the linear stability results published by Sun *et al.* [4]. The agreement between stability theory and the present numerical experiments is illustrated further in Fig. 8: the 'neutral stability' line on this figure was drawn from the data in Sun *et al.*'s Fig. 2 and, considering the miniscule size of that source, we estimate that the neutral stability line is accurate within $\pm 10\%$ (in order to collect Sun *et al.*'s data we first had to photographically blow up their Fig. 2).

The effect of bottom wall temperature

Noting that the porous layer contains a stably-stratified region situated above a potentially unstable region, Fig. 1, an important parameter of the natural convection phenomenon is the relative 'thickness' of the potentially unstable region. Since the temperature of the upper boundary is fixed at 0°C, the relative thickness of the potentially unstable region is controlled by the temperature of the bottom boundary T_H in the form of the ratio $(T_H - 3.98°C)/(3.98°C - 0°C)$. In the flow patterns illustrated so far, Figs. 4–6, the bottom wall temperature was set at 8°C: in the conduction regime this would translate into a potentially unstable region having the same thickness as the stably stratified upper region.

As the bottom temperature T_H approaches 3.98°C, i.e. as the potentially unstable region vanishes, it is reasonable to expect the disappearance of natural circulation. This behavior is confirmed by numerical experiments, as summarized in Fig. 9 which uses the Nusselt number Nu as a measure of natural convection intensity. At the Rayleigh number $Ra_p = 10^3$, the flow disappears rather abruptly as the bottom wall temperature T_H drops from 5.8 to 5.7°C (note that with pure conduction prevailing at $T_H = 5.7°C$, the potentially unstable region is almost half as thick as the stably stratified upper region). When the system is marginally in the convection regime, $T_H = 5.8°C$ (Fig. 10), the flow consists of rolls of nearly square cross-section occupying the lower half of the layer. Comparing Fig. 9 and Fig. 4 we find that as the bottom wall temperature increases from the onset level 5.8°C to 8°C the rolls become considerably taller in cross-section, as they become stronger and intrude vertically into the region that would have been occupied by stably stratified fluid.

The disappearance of convection as T_H decreases at constant Ra_p is reported also on Fig. 8. Note that the transition takes place at a temperature T_H higher than the minimum 3.98°C needed for the existence of a

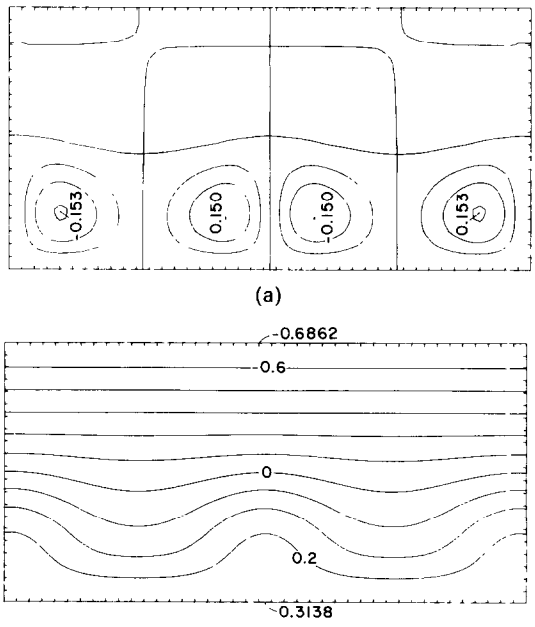

FIG. 10. Numerical solution for $A = 0.5$, $T_H = 5.8°C$, $Ra_p = 1000$: (a) streamlines ($\hat{\psi}$ = const.); (b) isotherms ($\hat{T}$ = const.).

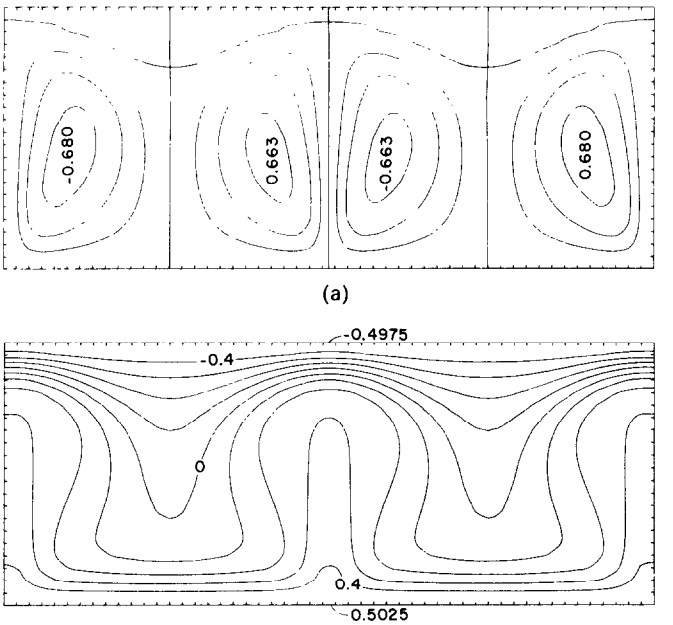

FIG. 11. Numerical solution for $A = 0.4$, $T_H = 8°C$, $Ra_p = 1000$: (a) streamlines ($\hat{\psi}$ = const.); (b) isotherms ($\hat{T}$ = const.).

potentially unstable region at the bottom of the porous layer.

The effect of geometric aspect ratio

In view of the numerical necessity to isolate out of the infinite porous layer only a section of length L, Fig. 1, it is important to examine the effect of L in other words, the effect of the presence of the two vertical adiabatic boundaries at $x = 0$ and L. The series of experiments that illustrate this effect were conducted in a porous layer with fixed boundary temperatures and height ($Ra_p = 10^3$, $T_H = 8°C$), by varying the length from $L = H$ to $6H$ (Table 1).

The flow and temperature patterns exhibited in Figs. 11 and 12 show that the lateral extent of the porous layer has a relatively weak impact on the local character

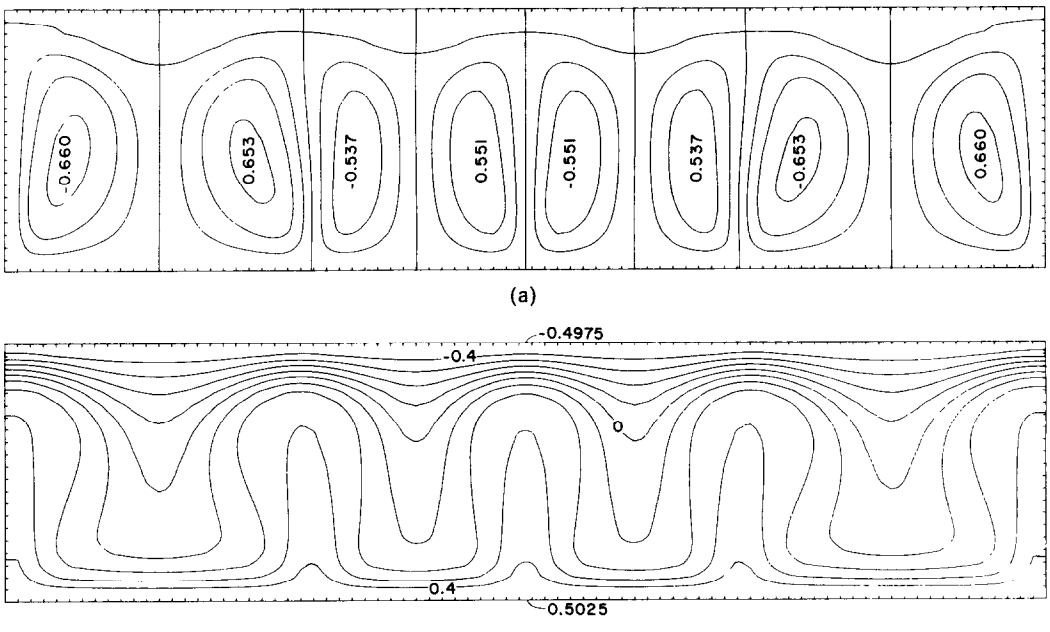

FIG. 12. Numerical solution for $A = 0.25$, $T_H = 8°C$, $Ra_p = 1000$: (a) streamlines ($\hat{\psi}$ = const.); (b) isotherms ($\hat{T}$ = const.).

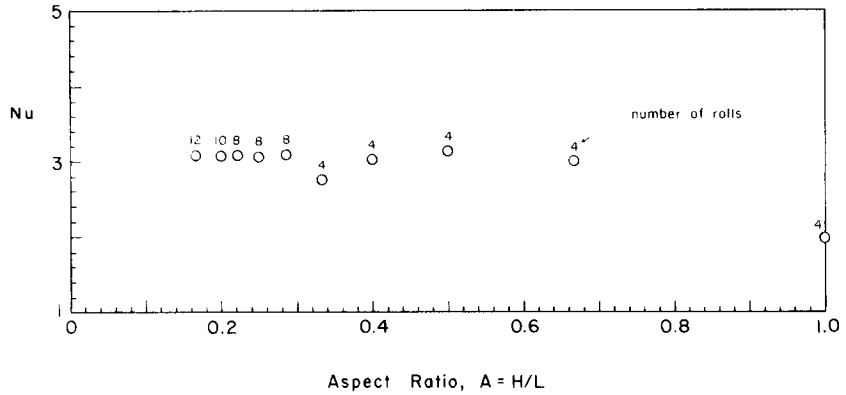

FIG. 13. The effect of aspect ratio A on the overall Nusselt number ($T_H = 8°C$, $Ra_p = 1000$).

of the flow. As the length L increases the rolls increase in number, however, their strength and individual height/thickness ratios remain largely insensitive to this change. The increase in the number of rolls takes place discretely as indicated via the Nusselt number in Fig. 13. The overall effect of aspect ratio H/L on Nu is small when Ra_p and T_H are held constant. Nevertheless, it is interesting to note that in the range $1/3 < H/L < 1$ where the flow consists of four rolls, the Nusselt number has a maximum. This is an indication that in the H/L range 1/3–1 there exists a particular geometry in which the four rolls fit best. Reducing the aspect ratio below this uptimum value results in the stretching of the two cells and in the formation of regions of relatively slower moving fluid, hence, the slight decrease in the Nusselt number. The stretching of each roll terminates abruptly below $H/L = 1/3$, and each roll is replaced by two counter-rotating rolls. The increased convection capability of the new flow (i.e. the disappearance of relatively slow moving fluid between stretched cells), is marked by a sudden jump in the Nusselt number.

The occurrence of a maximum Nusselt number at the point where each roll attains that special geometry that 'fits best' in the (H, L) porous layer selected for numerical analysis is emphasized in Fig. 14. When plotted against the average height/length ratio of an individual cell

$$\frac{H}{l} = \frac{H}{L/n} \tag{19}$$

all the Nusselt number data of Fig. 13 fall on a single curve that shows a distinct maximum around $H/l = 2$. (Note that in definition (19) n represents the number of rolls listed in Table 1 and Fig. 13.) The correlation of heat transfer data in the Nu–H/l plane demonstrates that the overall heat transfer rate is controlled by the geometric aspect ratio of the individual roll, and that there exists a natural (optimum) roll geometry that maximizes the overall heat transfer rate vertically across the porous layer.

In closing, we should point out that the simple parabolic density model (6) is highly accurate in the temperature range covered by this study. In a related

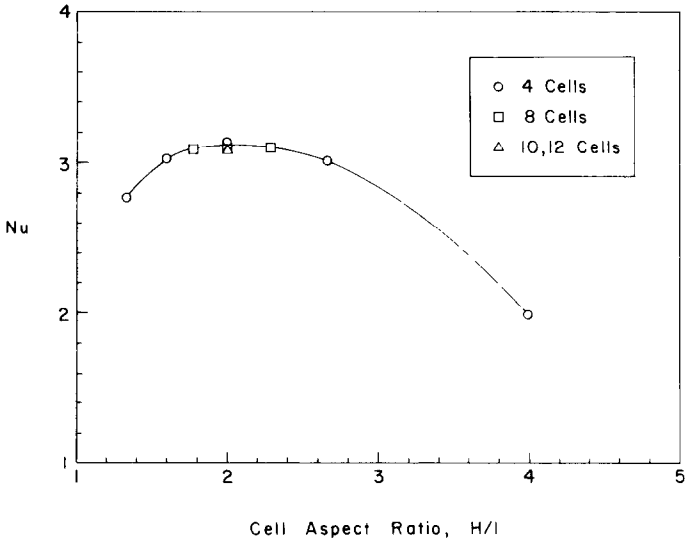

FIG. 14. Correlation of the results of Fig. 13, showing the maximum heat transfer rate associated with a certain cell aspect ratio, equation (19).

study of convection in cold water layers without porous matrix [16] we found that the numerical results based on model (6) were practically the same as those obtained using a more refined cubic model.

Acknowledgement—This research was supported by the National Science Foundation through Grant No. MEA-82-07779.

REFERENCES

1. S. L. Goren, On free convection in water at 4°C, *Chem. Engng Sci.* **21,** 515–518 (1966).
2. D. R. Moore and N. O. Weiss, Nonlinear penetrative convection, *J. Fluid Mech.* **61,** 553–581 (1973).
3. J. Boussinesq, *Theorie Analytique de la Chaleur*, Vol. 2, p. 172. Gauthier-Villars, Paris (1903).
4. Z. S. Sun, C. Tien and Y. C. Yen, Onset of convection in a porous medium containing liquid with a density maximum, *Proc. 4th Int. Heat Transfer Conf.*, Paris, Versailles, paper NC 2.11 (1972).
5. Y. C. Yen, Effects of density inversion on free convection heat transfer in a porous layer heated from below, *Int. J. Heat Mass Transfer* **17,** 1349–1356 (1974).
6. J. M. Ramilison and B. Gebhart, Buoyancy induced transport in porous media saturated with pure or saline water at low temperatures, *Int. J. Heat Mass Transfer* **23,** 1521–1530 (1980).
7. P. Cheng, Heat transfer in geothermal systems, *Adv. Heat Transfer* **14,** 1–105 (1979).
8. E. R. Lapwood, Convection of a fluid in a porous medium, *Proc. Camb. Phil. Soc.* **44,** 508–521 (1948).
9. M. A. Combarnous and S. A. Bories, Hydrothermal convection in saturated porous media, *Adv. Hydrosci.* **10,** 231–307 (1975).
10. R. J. Buretta and A. S. Berman, Convective heat transfer in a liquid saturated porous layer, *J. Appl. Mech.* **43,** 249–253 (1976).
11. J. W. Elder, Steady free convection in a porous medium heated from below, *J. Fluid Mech.* **27,** 29–48 (1967).
12. V. P. Gupta and D. D. Joseph, Bounds for heat transport in a porous layer, *J. Fluid Mech.* **57,** 491–514 (1973).
13. J. M. Strauss, Large amplitude convection in porous media, *J. Fluid Mech.* **64,** 51–63 (1974).
14. *CRC Handbook of Chemistry and Physics* (56th edn.). Chemical Rubber Company, Cleveland, Ohio (1975).
15. S. Patankar, *Numerical Heat Transfer and Fluid Flow*. Hemisphere, New York (1980).
16. K. R. Blake, D. Poulikakos and A. Bejan, Natural convection near 4°C in a horizontal water layer heated from below, *Phys. Fluids*, in press.

CONVECTION NATURELLE AUTOUR DE 4°C DANS UNE COUCHE POREUSE SATUREE D'EAU ET CHAUFFEE PAR LE BAS

Résumé—On rapporte une étude numérique de la convection naturelle bidimensionnelle dans une couche poreuse horizontale chauffée par le bas et saturée d'eau froide. Le maximum de densité à 3,98°C et la pression atmosphérique sont réalisés dans la couche, avec la surface supérieure maintenue à 0°C tandis que la face inférieure est entre 4 et 8°C. Trois séries séparées de simulations numériques précisent les effets de la température de la base, de la longueur horizontale de la couche sur le transfert thermique global perpendiculairement à la couche. Le domaine de ces expériences numériques est $200 < Ra_p < 10000$, $0{,}167 < H/L < 1$ et $4°C < T_H < 8°C$, où Ra_p, H/L et T_H sont le nombre de Rayleigh modifié Darcy pour un fluide à maximum de densité, le rapport hauteur/longueur et la température de la base. Les résultats numériques s'accordent bien avec les résultats de stabilité linéaire sur l'apparition de la convection.

FREIE KONVEKTION BEI 4°C IN EINER MIT WASSER ÜBERFLUTETEN SCHÜTTUNG, DIE VON UNTEN BEHEIZT WIRD

Zusammenfassung—Über die numerische Untersuchung der zweidimensionalen natürlichen Konvektion in einer waagerechten Schicht einer mit kaltem Wasser überfluteten, von unten beheizten Schüttung wird berichtet. Das Dichtemaximum des Wassers bei 3,98°C und Atmosphärendruck tritt in der Schicht auf, da die Oberseite bei 0°C gehalten und die Temperatur der Unterseite zwischen 4 und 8°C variiert wird. Drei getrennte Serien der numerischen Simulation zeigen den Einfluß der Rayleigh-Zahl, der Temperatur an der Unterseite und der horizontalen Ausdehnung der Schicht auf den Gesamtwärmedurchgang in vertikaler Richtung durch die Schüttung. Die numerischen Untersuchungen wurden für $200 < Ra_p < 10000$, $0{,}167 < H/L < 1{,}0$ und $4°C < T_H < 8°C$ durchgeführt. Dabei ist Ra_p die nach Darcy modifizierte Rayleigh-Zahl für Medien mit Dichtemaximum, H/L das geometrische Verhältnis von Höhe zu horizontaler Ausdehnung und T_H die Temperatur der unteren Begrenzungsfläche. Die numerischen Ergebnisse stimmen mit veröffentlichten Ergebnissen über die lineare Stabilität überein, was das Einsetzen der Konvektion betrifft.

ЕСТЕСТВЕННАЯ КОНВЕКЦИЯ В НАСЫЩЕННОМ ВОДОЙ ПОРИСТОМ НАГРЕВАЕМОМ СНИЗУ СЛОЕ ПРИ ТЕМПЕРАТУРЕ, БЛИЗКОЙ К 4 С

Аннотация—Проведено численное исследование двумерной естественной конвекции в горизонтальном пористом слое, нагреваемом снизу и насыщенном холодной водой. Максимум плотности воды, имеющий место при температуре 3,98 С и атмосферном давлении, находится внутри слоя, так как нижняя поверхность поддерживается при температуре 0 С, а верхняя при температуре, меняющейся в пределах от 4 до 8 С. Три отдельные серии численного моделирования подтверждают влияние числа Рэлея, температуры нижней поверхности и длины пористого слоя по горизонтали на суммарную интенсивность теплопереноса через слой в вертикальном направлении. Численные эксперименты проводились в диапазонах $200 < Ra_p < 10000$, $0{,}167 < H/L < 1$ и $4\ C < T_H < 8\ C$, где Ra_p, H/L и T_H – соответственно модифицированное по Дарси число Рэлея при максимальной плотности жидкости, отношение высоты слоя к его длине и температура нижней поверхности слоя. Полученные численные результаты согласуются с опубликованными данными об устойчивости по отношению к возникновению конвекции, полученными в линейной теории.